Ultrasmall and ultradense InGaN-based RGB monochromatic micro-light-emitting diode arrays by pixilation of conductive p-GaN

PHOTONICS Research

Ultrasmall and ultradense InGaN-based RGB monochromatic micro-light-emitting diode arrays by pixilation of conductive p-GaN

ZHE ZHUANG, DAISUKE IIDA, AND KAZUHIRO OHKAWA*

Computer, Electrical and Mathematical Sciences and Engineering (CEMSE) Division, King Abdullah University of Science and Technology (KAUST), Thuwal 23955-6900, Saudi Arabia
**Corresponding author: kazuhiro.ohkawa@kaust.edu.sa*

Received 5 August 2021; revised 5 October 2021; accepted 14 October 2021; posted 19 October 2021 (Doc. ID 439741); published 15 November 2021

We describe 5 μm squircle InGaN-based red, green, and blue (RGB) monochromatic micro-light-emitting diodes (μLEDs) with an interpitch of 4 μm by pixilation of conductive p-GaN using a H_2-plasma treatment. The p-GaN was passivated by H_2 plasma and prevented the current's injection into the InGaN quantum wells below. We observed that InGaN-based red μLEDs exhibited a broader full width at half-maximum and larger peak wavelength blueshift at 11.5–115 A/cm^2 than the green/blue μLEDs. The on-wafer light output power density of the red μLEDs at a wavelength of 632 nm at 115 A/cm^2 was approximately 936 mW/cm^2, the highest value reported thus far for InGaN-based red μLEDs. This value was comparable with that of the green/blue μLEDs at 11.5 A/cm^2, indicating that the red μLEDs can satisfy the requirement of high brightness levels for specific displays. The color gamut based on InGaN RGB μLEDs covered 83.7% to 75.9% of the Rec. 2020 color space in the CIE 1931 diagram at 11.5 to 115 A/cm^2.

https://doi.org/10.1364/PRJ.439741

1. INTRODUCTION

Owing to their high efficiency, brightness, and stability, InGaN-based micro-light-emitting diodes (μLEDs) have been considered as core devices in next-generation displays for a wide variety of applications, e.g., wall displays/televisions, smartphones/watches, head-up displays, pico-projectors, and augmented-reality (AR) glasses [1–3]. The full-color μLED displays require integration of red, green, and blue (RGB) μLEDs (R: AlGaInP; G and B: InGaN) on the same panel by pick-and-place technologies. However, the different material systems might cause mismatched far-field radiation patterns for RGB μLEDs [4], leading to a negative visual experience.

Most importantly, the high surface recombination velocities and long carrier diffusion lengths for AlGaInP materials will drastically reduce the efficiency of red μLEDs when the μLED dimensions shrink below 25 μm [5–7]. As a result, InGaN is gathering growing interest as an alternative red μLED candidate.

Despite the good performance of green/blue μLEDs, InGaN-based red μLEDs require an increase in the In-content in InGaN quantum wells (QWs), which will cause significant reduction in efficiency due to the degraded crystal quality of high-In-content InGaN QWs [8]. To solve this problem, special substrates/templates were proposed for high-In-content InGaN growth, such as InGaNOS [9], $ScAlMgO_4$ (0001) [10], and porous GaN [11]. Our group grows high-In-content InGaN QWs by micro-flow-channel metalorganic vapor-phase epitaxy (MOVPE) [12] on sapphire substrates, and the red μLEDs [13] exhibited good efficiencies compared with other works [9,11]. However, the large blueshift of the peak wavelength for InGaN red μLEDs will make them look yellow or orange at high current densities, which cannot satisfy the requirement of the high dynamic operation range for microdisplays (like seamless AR glasses). Therefore, developing InGaN red μLEDs that operate in a high dynamic current density range is necessary.

Besides, ultrasmall (<10 μm) InGaN μLEDs are usually fabricated by mesa etching, which physically removes the nitride materials and defines the dimensions of μLEDs [14,15]. This method is the most popular pixilation technique but introduces sidewall damage and reduces device efficiencies [16–18]. Although it is possible to remove damage by chemical etching [19], the efficiencies of InGaN green/blue μLEDs still decrease as the dimension shrinks below 10 μm [20]. Meanwhile, ultra-small (<10 μm) red μLEDs are seldom reported for both InGaN and AlGaInP materials [11].

To avoid the drawbacks of mesa etching, the research group from Samsung Ltd. proposed a new pixilation strategy [21] in which it tailored ion implantation to fabricate pixelated InGaN

μLEDs and demonstrated high (2000–5000) pixels per inch (PPI) μLED displays with monolithically integrated thin-film transistor pixel circuits. However, this tailored ion implantation should be precisely controlled, which complicates the fabrication process. A simple strategy is more favorable for this kind of pixilation process.

In this work, we describe 5 μm squircle InGaN-based RGB monochromatic μLEDs with an interpitch of 4 μm using H_2-plasma treatment for pixilation of conductive p-GaN. We examined the current-voltage curves to investigate the passivated p-GaN contacts and the electrical performances of the RGB μLEDs. The electroluminescence (EL) properties of the RGB monochromatic μLEDs, such as spectra and light output power (LOP), were investigated. Finally, we evaluated the uniformity and distinctiveness of the RGB μLEDs qualitatively and determined their color gamut in the CIE 1931 diagram.

2. EXPERIMENTAL DETAILS

InGaN-based red LED epitaxial wafers were grown on *c*-plane patterned sapphire substrates by MOVPE. Our previous work reported the epitaxial structures, which utilized the thick GaN template [22], hybrid InGaN QWs [23], and AlN/AlGaN hybrid barrier layers [24]. These epi-structures were designed to adjust strain, which helps to improve the crystal quality of InGaN red QWs. The n-type layer in our red LED structure is n-$Al_{0.03}Ga_{0.97}N$, which could realize extremely low resistivity by high Si doping [25]. The growth parameters were similar to those of our previous work [22], but we adjusted the growth temperature for high-In-content InGaN red QWs. The InGaN-based green/blue LED epitaxial wafers were purchased from a commercial supplier. The green/blue commercial epi-wafers can guarantee uniformity and are also suitable to be regarded as the reference samples because they are available for all research groups. Note that the n-type layer in the commercial green/blue LED structures is n-GaN.

The schematic of fabrication processes via pixilation of the conductive p-GaN is shown in Fig. 1. The indium tin oxide (ITO) micro-pillars arrays (20 × 20) were fabricated by standard lithography and a lift-off process in sequence [Fig. 1(a)]. The micro-pillars were squircle, with a width of 5 μm. The average area of the single 5 μm squircle was 21.66 μm^2. The interpitch between the adjacent ITO micro-pillars was 4 μm. The ohmic contacts between ITO micro-pillars and p-GaN were formed by the rapid two-step annealing process [26]. Then, the exposed p-GaN areas were treated with H_2 plasma at 300°C for 2 min. Due to the high-temperature treatment, the H atoms would be not only captured by the p-GaN surface but also diffuse inside the p-GaN layer [27,28]. As a result, the H atoms were bonded to the p-type dopant Mg atoms and passivated the exposed p-GaN, as shown in Fig. 1(b). Finally, an additional ITO layer was used to connect all ITO micro-pillars and the Cr/Au served as the n- and p-electrodes [Fig. 1(c)]. To improve transparency and conductivity of this additional ITO layer, we carried out a two-step rapid annealing process before depositing Cr/Au electrodes. We also fabricated blue LEDs without ITO micro-pillars for comparison. The blue LEDs underwent the same processes in Figs. 1(b) and 1(c) to investigate the current injection of the passivated p-GaN areas.

The InGaN-based RGB monochromatic μLEDs were characterized at a probe station using a semiconductor parameter analyzer at room temperature. The EL properties were measured by the on-wafer testing, which had a similar configuration to the previous work [29]. A CCD camera installed on the microscope at the probe station was used to capture the emission patterns of these RGB monochromatic μLEDs.

3. RESULTS AND DISCUSSION

We first examined the contacts between the passivated p-GaN and the ITO layer. The absolute current of the blue LED with the passivated p-GaN was measured under the applied voltage from −4 to 8 V, as shown in Fig. 2. The measured current of the blue LED was less than 1 μA even at the forward bias of 8 V, demonstrating the typical Schottky contact between the passivated p-GaN and the ITO layer. Therefore, we could realize the μLEDs by the pixilation of the conductive p-GaN, as explained in Fig. 1.

The absolute current-voltage ($|I| - V$) curves of the InGaN RGB monochromatic μLED arrays (20 × 20) are plotted in Fig. 2 under the different applied voltages. The absolute

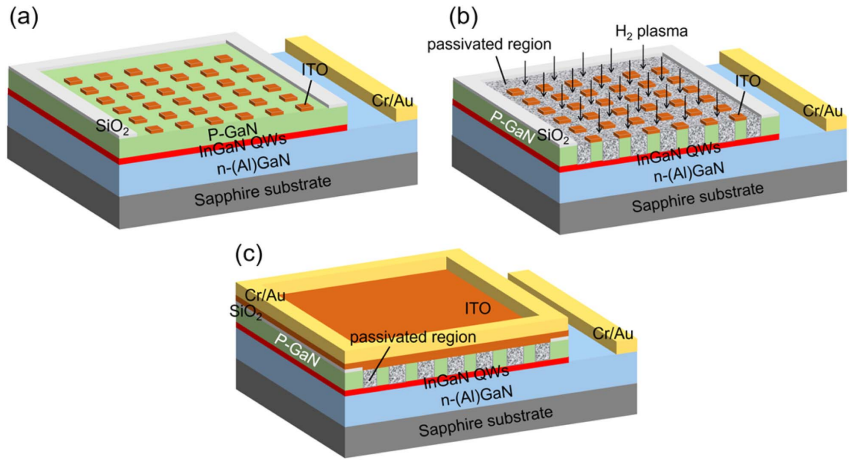

Fig. 1. Schematics of fabrication processes for InGaN-based RGB monochromatic μLEDs by pixilation of conductive p-GaN.

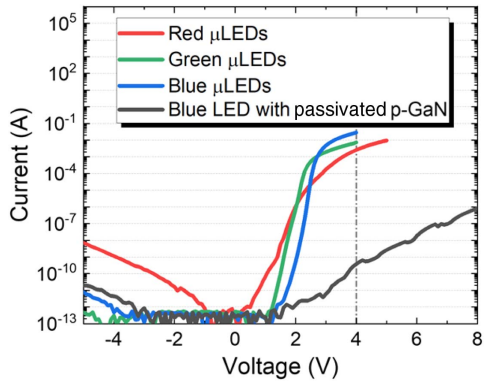

Fig. 2. $|I| - V$ curves of InGaN-based RGB μLEDs and the blue LED with passivated p-GaN.

current is plotted on a logarithmic scale. At the forward voltage, the $|I| - V$ characteristics of RGB monochromatic μLEDs exhibited similar behavior. The curves could be separated into two linear parts with different slopes on the semi-logarithmic scale. The two linear parts of the $|I| - V$ curves in forward bias were the same as that of the μLEDs by mesa etching [13,29]. The turn-on voltage, usually defined as the transition point between the two linear parts, was between 2.0 and 3.0 V for these RGB monochromatic μLEDs. The green μLEDs exhibited the lowest turn-on voltage compared with the blue and red μLEDs.

In addition, we noticed that the currents at 4 V for the RGB μLEDs were above 10^{-3} A, more than six orders of magnitude larger than that for the blue LED with passivated p-GaN. This result further illustrates that the current could only pass through the activated p-GaN areas covered by ITO micro-pillars for the RGB monochromatic μLED arrays. As a result, we could calculate the current density by using the measured currents divided by the ITO micro-pillar area. At around 12 A/cm^2, the forward voltage of RGB monochromatic μLED arrays was around 3.6, 2.7, and 2.7 V, respectively.

At the reverse voltage, the reverse current remained constant for green/blue monochromatic μLEDs. However, the reverse current for the red μLEDs increased after the reverse voltage was above −1 V. This reverse current increase implied that some leakage channels existed in the InGaN red μLEDs, presumably caused by defects in the InGaN QWs [30].

Figure 3(a) shows the EL spectra of the RGB monochromatic μLEDs at 11.5 to 115 A/cm^2. The EL spectra of the red μLEDs were multiplied by tenfold in the figure. We observed that all EL spectra of the green/blue monochromatic μLEDs exhibited single peaks. However, the red μLEDs had a tiny additional peak located in the wavelength range of 460–480 nm. We presumed that this additional peak was mainly caused by the indium phase separation in high-In-content InGaN QWs [31,32].

The peak wavelengths of the RGB monochromatic μLEDs exhibited the blueshift as the current density increased in Fig. 3(a). However, the blueshift values from 11.5 to 115 A/cm^2 were quite different for the RGB monochromatic μLEDs. The blue and green μLEDs showed a slight blueshift of the peak wavelength within 4 nm. However, the red μLED had a blueshift of approximately 34 nm from the peak wavelength of 666 nm at 11.5 A/cm^2 to 632 nm at 115 A/cm^2. This blueshift for the red μLED is similar to our previous amber μLEDs [29] and was mainly caused by the strong QCSE in the high-In-content InGaN QWs.

We also extracted and compared the FWHMs of the RGB monochromatic μLEDs, as shown in Fig. 3(b). The FWHMs at 11.5–115 A/cm^2 were around 20–22 nm for the blue μLEDs. But this became broader, to 28–31 and 72–81 nm, for the green and red μLEDs, respectively. This result was reasonable because the In fluctuation would be increased in the high-In-content InGaN QWs. Besides, the FWHMs of the RGB monochromatic μLEDs became broader as the current density increased, which originated from the generated heat under the high current density operation [31]. The heat was usually generated at the vicinity of defects [33], so the higher defect densities in the red μLEDs would generate more heat and make the value of FWHM larger compared with the green/blue monochromatic μLEDs.

The on-wafer LOP density can be used to evaluate the brightness of μLEDs. Figure 4 shows that the calculated on-wafer LOP density of green μLEDs is slightly lower than that of blue μLEDs. However, the LOP density of the red μLEDs is almost one order of magnitude lower than that of the green/blue μLEDs at the same current density. Besides, the LOP density of the red μLEDs decreased faster as the current density decreased when compared with the green/blue μLEDs. The phenomenon can be explained by the dominant

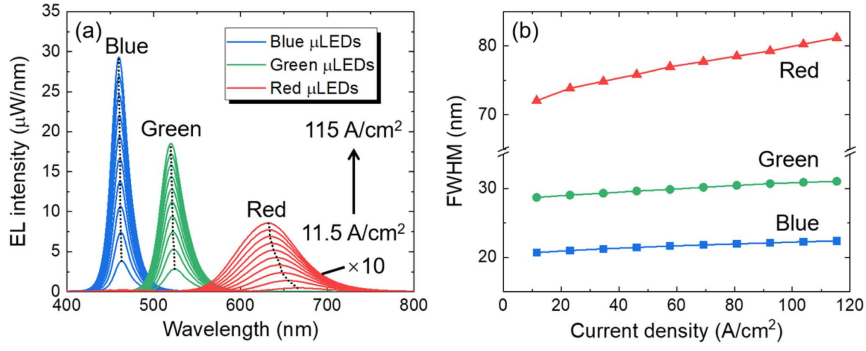

Fig. 3. (a) EL spectra. (b) FWHM of RGB monochromatic μLEDs at 11.5 to 115 A/cm^2.

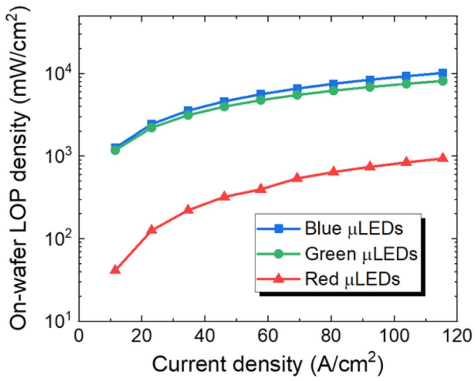

Fig. 4. On-wafer LOP density of RGB monochromatic μLEDs at different current densities.

Shockley–Read–Hall (SRH) recombination at lower current densities. Compared with green/blue μLEDs, red μLEDs have more defects in the active region. These defects serve as the SRH recombination centers and suppress the radiative recombination, especially at the lower current densities [34]. Therefore, less percent of carriers contribute to the light output and result in further reduction of the LOP density for red μLEDs as the current density decreases.

Because of the lower LOP density, the red μLEDs require to be operated at a higher current density to achieve a similar brightness to that of the green/blue μLEDs. Generally, AR head-mounted displays need to achieve very high brightness ($\sim 1 \times 10^5$ cd/m^2), which requires the blue μLEDs operating at ~10 A/cm^2 [21]. To achieve a similar brightness, we estimated that the red μLEDs should exhibit a similar level of the LOP density to the blue μLEDs. As a result, we found that red μLEDs needed to be operated at ~115 A/cm^2 in Fig. 4, one order of magnitude higher than the operated current density for blue μLEDs (11.5 A/cm^2 in Fig. 4). Fortunately, even at such a high current density, our red μLEDs still have a peak wavelength of 632 nm [Fig. 3(a)], which guarantees the emission located at the red region. Therefore, we conclude that our red μLEDs can satisfy the very high brightness requirement for AR displays.

We also compared the performance of the red μLEDs with other works [9,11,13,35,36]. As shown in Table 1, the red μLEDs in this work realized the highest current density at the emission wavelength around 630 nm. As a result, the LOP density of the red μLEDs reaches approximately 936 mW/cm^2, which is the highest reported value so far for InGaN-based red μLEDs.

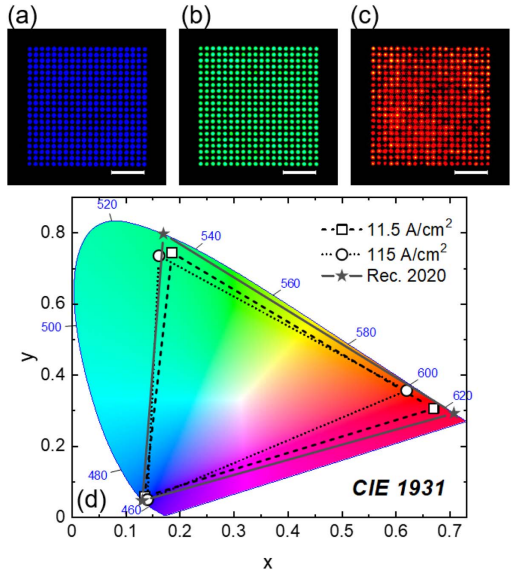

Fig. 5. (a)–(c) EL emission images of RGB monochromatic μLED arrays at 115 A/cm^2. The scale bar in the inset is 50 μm. (d) CIE 1931 diagram of RGB monochromatic μLED arrays at 11.5 and 115 A/cm^2.

Figures 5(a)–5(c) show the EL emission images of RGB monochromatic μLED arrays at 115 A/cm^2. We adjusted the exposure time for the CCD camera to capture these images. The clear RGB μLED pixels in these figures imply that the pixilation of the conductive p-GaN in Fig. 1 worked well to realize ultrasmall μLEDs. Besides, Fig. 5(c) implies that our red μLEDs at 115 A/cm^2 look "red," demonstrating the possibility of our red μLEDs to work as a "red color" for high brightness requirement. However, compared with the uniform luminescence of green/blue monochromatic μLED arrays, some bright and dark pixels could be observed for the red μLED arrays. This luminescence nonuniformity was caused by many defects in the red QWs [26,31], which should be further reduced in the future.

We also calculated the coordinates of RGB monochromatic μLEDs at 11.5 and 115 A/cm^2 in the CIE 1931 diagram [Fig. 5(d)]. The primary RGB colors in Rec. 2020 are plotted as stars for comparison. Due to the blueshift of the emission wavelength in Fig. 3(a), the positions in CIE 1931 would move counterclockwise for green and red μLEDs but almost remain constant for blue μLEDs. The color gamut by the RGB monochromatic μLEDs covered 83.7% to 75.9% of the Rec. 2020 color space at 11.5 to 115 A/cm^2. The coverage values are

Table 1. Comparison of LOP Density for InGaN-Based Red μLEDs

Affiliation	Peak Wavelength (nm)	Current Density (A/cm^2)	LOP Density (mW/cm^2)
KAUST (this work)	632	115	936
KAUST [13]	626	4	29
KAUST [35]	630	50	176
UCSB [11]	632	10	40
Univ. of Grenoble-Alpes [9]	630	0.8	0.4
Plessey [36]	630	10	—

quite comparable with RGB μLEDs using quantum dot color converters [37,38].

4. CONCLUSION AND PROSPECT

In summary, here we have demonstrated that the p-GaN was passivated after H_2-plasma treatment and would form a Schottky contact with the ITO layer, which prevented the current injection into InGaN QWs. We utilized this pixilation method to realize 5 μm squircle InGaN-based RGB monochromatic μLEDs and maintained the good distinctiveness of the ultrasmall μLED pixels. A broader FWHM (72–81 nm) and a larger peak wavelength blueshift from 666 to 632 nm at 11.5–115 A/cm^2 were observed for the red μLEDs. The on-wafer LOP density of the red μLEDs was obtained as 936 mW/cm^2, which is the highest reported value thus far for InGaN-based red μLEDs. However, the on-wafer LOP density of the red μLEDs was still lower than that of green/blue μLEDs by one order of magnitude, which required higher operation current densities for red μLEDs to achieve similar brightness. The color gamut based on InGaN RGB monochromatic μLEDs covered 83.7% and 75.9% of the Rec. 2020 color space in CIE 1931 at 11.5 and 115 A/cm^2, respectively.

To realize full-color displays, the research group from Samsung Ltd. utilized the pixilation of blue μLEDs by ion implantation and chose quantum dot color converters for red/green μLEDs [21]. They avoided the mass transfer process and realized the prototype of micro-displays. In the case of RGB monochromatic μLEDs, the full-color displays generally need to assemble individual RGB μLEDs side-by-side via mass transfer. But this integration method is not suitable for the proposed pixilation method in this work. Another approach is vertically stacking the monochromatic μLED arrays, which was demonstrated by Lee *et al.* for a dual-color μLED display [39] and by Yadavalli *et al.* for full-color μLED displays (R: AlGaInP; G and B: InGaN) [40]. Therefore, we can expect that this vertical stacking method can be used for integration of our pixelated RGB monochromatic μLED arrays for full-color ultrahigh-brightness and ultrahigh-definition displays in the future.

Funding. King Abdullah University of Science and Technology (BAS/1/1676-01-01).

Acknowledgment. The fabrication processes in this work were supported by Nanofabrication Core Labs in KAUST.

Disclosures. The authors declare no conflicts of interest.

Data Availability. Data underlying the results presented in this paper are not publicly available at this time but may be obtained from the authors upon reasonable request.

REFERENCES

1. Z. Chen, S. Yan, and C. Danesh, "MicroLED technologies and applications: characteristics, fabrication, progress, and challenges," J. Phys. D **54**, 123001 (2021).
2. H. S. Wasisto, J. D. Prades, J. Gülink, and A. Waag, "Beyond solid-state lighting: miniaturization, hybrid integration, and applications of GaN nano- and micro-LEDs," Appl. Phys. Rev. **6**, 041315 (2019).
3. P. J. Parbrook, B. Corbett, J. Han, T.-Y. Seong, and H. Amano, "Micro-light emitting diode: from chips to applications," Laser Photon. Rev. **15**, 2000133 (2021).
4. F. Gou, E.-L. Hsiang, G. Tan, P.-T. Chou, Y.-L. Li, Y.-F. Lan, and S.-T. Wu, "Angular color shift of micro-LED displays," Opt. Express **27**, A746–A757 (2019).
5. J.-T. Oh, S.-Y. Lee, Y.-T. Moon, J. H. Moon, S. Park, K. Y. Hong, K. Y. Song, C. Oh, J.-I. Shim, H.-H. Jeong, J.-O. Song, H. Amano, and T.-Y. Seong, "Light output performance of red AlGaInP-based light emitting diodes with different chip geometries and structures," Opt. Express **26**, 11194–11200 (2018).
6. M. S. Wong, J. A. Kearns, C. Lee, J. M. Smith, C. Lynsky, G. Lheureux, H. Choi, J. Kim, C. Kim, S. Nakamura, J. S. Speck, and S. P. DenBaars, "Improved performance of AlGaInP red micro-light-emitting diodes with sidewall treatments," Opt. Express **28**, 5787–5793 (2020).
7. S. Sinha, F. G. Tarntair, C. H. Ho, Y. R. Wu, and R. H. Horng, "Investigation of electrical and optical properties of AlGaInP red vertical micro-light-emitting diodes with Cu/Invar/Cu metal substrates," IEEE Trans. Electron Devices **68**, 2818–2822 (2021).
8. B. Damilano and B. Gil, "Yellow-red emission from (Ga,In)N heterostructures," J. Phys. D **48**, 403001 (2015).
9. A. Dussaigne, F. Barbier, B. Damilano, S. Chenot, A. Grenier, A. M. Papon, B. Samuel, B. B. Bakir, D. Vaufrey, J. C. Pillet, A. Gasse, O. Ledoux, M. Rozhavskaya, and D. Sotta, "Full InGaN red light emitting diodes," J. Appl. Phys. **128**, 135704 (2020).
10. T. Ozaki, M. Funato, and Y. Kawakami, "Red-emitting $In_xGa_{1-x}N$/$In_yGa_{1-y}N$ quantum wells grown on lattice-matched $In_yGa_{1-y}N$/$ScAlMgO_4$(0001) templates," Appl. Phys. Express **12**, 011007 (2019).
11. S. S. Pasayat, C. Gupta, M. S. Wong, R. Ley, M. J. Gordon, S. P. DenBaars, S. Nakamura, S. Keller, and U. K. Mishra, "Demonstration of ultra-small <10 μm) 632 nm red InGaN micro-LEDs with useful on-wafer external quantum efficiency (>0.2%) for mini-displays," Appl. Phys. Express **14**, 011004 (2020).
12. K. Ohkawa, T. Watanabe, M. Sakamoto, A. Hirako, and M. Deura, "740-nm emission from InGaN-based LEDs on *c*-plane sapphire substrates by MOVPE," J. Cryst. Growth **343**, 13–16 (2012).
13. Z. Zhuang, D. Iida, and K. Ohkawa, "Investigation of InGaN-based red/green micro-light-emitting diodes," Opt. Lett. **46**, 1912–1915 (2021).
14. H. Yu, M. H. Memon, D. Wang, Z. Ren, H. Zhang, C. Huang, M. Tian, H. Sun, and S. Long, "AlGaN-based deep ultraviolet micro-LED emitting at 275 nm," Opt. Lett. **46**, 3271–3274 (2021).
15. J. Yu, T. Tao, B. Liu, F. Xu, Y. Zheng, X. Wang, Y. Sang, Y. Yan, Z. Xie, S. Liang, D. Chen, P. Chen, X. Xiu, Y. Zheng, and R. Zhang, "Investigations of sidewall passivation technology on the optical performance for smaller size GaN-based micro-LEDs," Crystals **11**, 403 (2021).
16. S. S. Konoplev, K. A. Bulashevich, and S. Y. Karpov, "From large-size to micro-LEDs: scaling trends revealed by modeling," Phys. Status Solidi A **215**, 1700508 (2018).
17. P. F. Tian, J. J. D. McKendry, Z. Gong, B. Guilhabert, I. M. Watson, E. D. Gu, Z. Z. Chen, G. Y. Zhang, and M. D. Dawson, "Size-dependent efficiency and efficiency droop of blue InGaN micro-light emitting diodes," Appl. Phys. Lett. **101**, 231110 (2012).
18. J. Kou, C.-C. Shen, H. Shao, J. Che, X. Hou, C. Chu, K. Tian, Y. Zhang, Z.-H. Zhang, and H.-C. Kuo, "Impact of the surface recombination on InGaN/GaN-based blue micro-light emitting diodes," Opt. Express **27**, A643–A653 (2019).
19. M. S. Wong, C. Lee, D. J. Myers, D. Hwang, J. A. Kearns, T. Li, J. S. Speck, S. Nakamura, and S. P. DenBaars, "Size-independent peak efficiency of III-nitride micro-light-emitting-diodes using chemical treatment and sidewall passivation," Appl. Phys. Express **12**, 097004 (2019).
20. J. M. Smith, R. Ley, M. S. Wong, Y. H. Baek, J. H. Kang, C. H. Kim, M. J. Gordon, S. Nakamura, J. S. Speck, and S. P. DenBaars, "Comparison of size-dependent characteristics of blue and green

InGaN microLEDs down to 1 μm in diameter," Appl. Phys. Lett. **116**, 071102 (2020).
21. J. Park, J. H. Choi, K. Kong, J. H. Han, J. H. Park, N. Kim, E. Lee, D. Kim, J. Kim, D. Chung, S. Jun, M. Kim, E. Yoon, J. Shin, and S. Hwang, "Electrically driven mid-submicrometre pixilation of InGaN micro-light-emitting diode displays for augmented-reality glasses," Nat. Photonics **15**, 449–455 (2021).
22. D. Iida, Z. Zhuang, P. Kirilenko, M. Velazquez-Rizo, M. A. Najmi, and K. Ohkawa, "633-nm InGaN-based red LEDs grown on thick underlying GaN layers with reduced in-plane residual stress," Appl. Phys. Lett. **116**, 162101 (2020).
23. D. Iida, K. Niwa, S. Kamiyama, and K. Ohkawa, "Demonstration of InGaN-based orange LEDs with hybrid multiple-quantum-wells structure," Appl. Phys. Express **9**, 111003 (2016).
24. D. Iida, S. Lu, S. Hirahara, K. Niwa, S. Kamiyama, and K. Ohkawa, "Enhanced light output power of InGaN-based amber LEDs by strain-compensating AlN/AlGaN barriers," J. Cryst. Growth **448**, 105–108 (2016).
25. T. Sugiyama, D. Iida, T. Yasuda, M. Iwaya, T. Takeuchi, S. Kamiyama, and I. Akasaki, "Extremely low-resistivity and high-carrier-concentration Si-doped $Al_{0.05}Ga_{0.95}N$," Appl. Phys. Express **6**, 121002 (2013).
26. Z. Zhuang, D. Iida, P. Kirilenko, M. Velazquez-Rizo, and K. Ohkawa, "Optimal ITO transparent conductive layers for InGaN-based amber/red light-emitting diodes," Opt. Express **28**, 12311–12321 (2020).
27. A. Y. Polyakov, N. B. Smirnov, A. V. Govorkov, K. H. Baik, S. J. Pearton, B. Luo, F. Ren, and J. M. Zavada, "Hydrogen plasma passivation effects on properties of p-GaN," J. Appl. Phys. **94**, 3960–3965 (2003).
28. H. Fu, K. Fu, H. Liu, S. R. Alugubelli, X. Huang, H. Chen, J. Montes, T.-H. Yang, C. Yang, J. Zhou, F. A. Ponce, and Y. Zhao, "Implantation- and etching-free high voltage vertical GaN p–n diodes terminated by plasma-hydrogenated p-GaN: revealing the role of thermal annealing," Appl. Phys. Express **12**, 051015 (2019).
29. Z. Zhuang, D. Iida, M. Velazquez-Rizo, and K. Ohkawa, "606-nm InGaN amber micro-light-emitting diodes with an on-wafer external quantum efficiency of 0.56%," IEEE Electron Device Letters **42**, 1029–1032 (2021).
30. T. Zhi, T. Tao, B. Liu, Z. Xie, P. Chen, and R. Zhang, "Reverse leakage current characteristics of GaN/InGaN multiple quantum-wells blue and green light-emitting diodes," IEEE Photon. J. **8**, 1601606 (2016).
31. Z. Zhuang, D. Iida, and K. Ohkawa, "Effects of size on the electrical and optical properties of InGaN-based red light-emitting diodes," Appl. Phys. Lett. **116**, 173501 (2020).
32. J. I. Hwang, R. Hashimoto, S. Saito, and S. Nunoue, "Development of InGaN-based red LED grown on (0001) polar surface," Appl. Phys. Express **7**, 071003 (2014).
33. S. Okamoto, N. Saito, K. Ito, B. Ma, K. Morita, D. Iida, K. Ohkawa, and Y. Ishitani, "Energy transport analysis in a $Ga_{0.84}In_{0.16}N$/GaN heterostructure using microscopic Raman images employing simultaneous coaxial irradiation of two lasers," Appl. Phys. Lett. **116**, 142107 (2020).
34. D. S. Meyaard, Q. Shan, J. Cho, E. F. Schubert, S.-H. Han, M.-H. Kim, C. Sone, S. J. Oh, and J. K. Kim, "Temperature dependent efficiency droop in GaInN light-emitting diodes with different current densities," Appl. Phys. Lett. **100**, 081106 (2012).
35. Z. Zhuang, D. Iida, M. Velazquez-Rizo, and K. Ohkawa, "630-nm red InGaN micro-light-emitting diodes (<20 μm × 20 μm) exceeding 1 mW/mm^2 for full-color micro-displays," Photon. Res. **9**, 1796–1802 (2021).
36. Y. Chen, "Plessey achieves native red InGaN LEDs on silicon for full color micro LED displays," https://www.ledinside.com/news/2019/12/plessey_ingan_red_led_microled (2019).
37. J.-H. Kang, B. Li, T. Zhao, M. A. Johar, C.-C. Lin, Y.-H. Fang, W.-H. Kuo, K.-L. Liang, S. Hu, S.-W. Ryu, and J. Han, "RGB arrays for micro-light-emitting diode applications using nanoporous GaN embedded with quantum dots," ACS Appl. Mater. Interfaces **12**, 30890–30895 (2020).
38. S.-W. H. Chen, Y.-M. Huang, K. J. Singh, Y.-C. Hsu, F.-J. Liou, J. Song, J. Choi, P.-T. Lee, C.-C. Lin, Z. Chen, J. Han, T. Wu, and H.-C. Kuo, "Full-color micro-LED display with high color stability using semipolar (20-21) InGaN LEDs and quantum-dot photoresist," Photon. Res. **8**, 630–636 (2020).
39. C.-M. Kang, D.-J. Kong, J.-P. Shim, S. Kim, S.-B. Choi, J.-Y. Lee, J.-H. Min, D.-J. Seo, S.-Y. Choi, and D.-S. Lee, "Fabrication of a vertically-stacked passive-matrix micro-LED array structure for a dual color display," Opt. Express **25**, 2489–2495 (2017).
40. K. Yadavalli, C.-L. Chuang, and H. El-Ghoroury, "Monolithic and heterogeneous integration of RGB micro-LED arrays with pixel-level optics array and CMOS image processor to enable small form-factor display applications," Proc. SPIE **11310**, 113100Z (2020).